

Visualization Research Center (VISUS)

University of Stuttgart
Allmandring 19
D-70569 Stuttgart

Bachelorarbeit

A VR-based Training System for an Ankle Surgery

Duc Anh Nguyen

Course of Study:	Softwaretechnik
Examiner:	Prof. Dr. Michael Sedlmair
Supervisor:	Xingyao Yu, M.Sc. Liang Zhou, Prof. Ph.D.
Commenced:	August 2, 2021
Completed:	March 2, 2022

Abstract

The supramalleolar osteotomy is a surgery, which aims to correct ankle osteoarthritis. Surgeons specializing in osteotomies regularly need to make accurate and precise cuts to a patient's bone with tools like an oscillating bone saw. In order to acquire the knowledge and skills to perform the real ankle surgery, they need to watch tutorials and practice on physical test models beforehand. In this work, we create a training system for the supramalleolar osteotomy in virtual reality. This includes the implementation of a bone cutting simulation and a post-analysis tool to evaluate the performance. A simple cut for this type of surgery requires the knowledge of its starting point, orientation, and current coverage. Furthermore, we design different concepts for visualizations, which aim to provide guidance, assistance, and feedback to the trainee surgeon during the operation. A preliminary study with a medical expert investigates the performance regarding the cut accuracy of each design. The study showed that the overall usage of those designed guidance visualizations improved the user's confidence during the operation. One key observation was that visualization directly positioned onto the cutting region performed better than the ones which were further away.

Contents

1	Introduction	13
2	Related Work	15
3	Background: Supramalleolar Osteotomy	17
3.1	Closing Wedge	18
3.2	Opening Wedge	18
4	Design Space	19
4.1	Base	20
4.2	Depth	21
4.3	Orientation	23
4.4	Tracking the Cut and Post-Analysis	26
5	Preliminary Study	29
5.1	Accuracy	29
5.2	Study Design	36
5.3	Evaluation	36
6	Discussion	39
7	Conclusion	41
	Bibliography	43

List of Figures

3.1	Closing Wedge X-Ray	17
3.2	Closing Wedge Procedure	18
3.3	Opening Wedge Procedure	18
4.1	Base Visualization	20
4.2	On-Cut-Visualization	21
4.3	Static-View-Visualization	22
4.4	Radial-Visualization	23
4.5	Line-Projection-Visualization	24
4.6	Line-Caster-Visualization	25
4.7	Training System Functionalities	26
4.8	Evaluation Mesh	26
4.9	Rotated cutting mesh to allow for a better view on the deviation.	27
5.1	Example deviation from the cutting plane.	29
5.2	Minimum and maximum deviations of an example deviation line.	30
5.3	Minimum and maximum deviations for the positive side.	31
5.4	Minimum and maximum deviations for the negative side.	32
5.5	Example for depth of a made cut and the target boundary curve.	33
5.6	Minimum and maximum depth with sampled points on the made cut.	34
5.7	Minimum and maximum depth for overshooting points.	35
5.8	Minimum and maximum depth for undershooting points.	35
5.9	Average deviation of all tested prototypes.	36
5.10	Maximum deviation of all tested prototypes.	37
5.11	Average distances to the target boundary curve of all tested prototypes.	38
5.12	Maximum distances to the target boundary curve of all tested prototypes.	38

List of Tables

4.1	Combinations of different visualizations	19
-----	--	----

Acronyms

AR Augmented Reality. 15

HMD Head Mounted Display. 15

VR Virtual Reality. 13

1 Introduction

In the field of surgery, every movement in the operation must be very meticulous and accurate. In osteotomies, usually they use very powerful hand-held oscillating saws to perform cuts on bones. Even the slightest error might have undesirable consequences. That is why a qualified surgeon needs to have a reliable estimation of the spatial geometry of the patients' bodies. In order to achieve that kind of qualification, they need to practice a lot on physical models before they can perform the real ankle surgery. In a conventional setting, trainees rely on instructions, feedback, and evaluation of an experienced surgeon, which is generally very resource and time-consuming.

Virtual Reality (VR) has the potential to lower the learning curve and accelerate the skill acquisition [RK05]. Through different visualizations, VR can offer a lot of helpful insight during training sessions. We can design visualizations that offer real-time feedback and instructions, such as indicators for wrong cuts or a system, which shows the overall progression of the operation. Because these visualizations are in a virtual environment, the possibilities for designs are less constrained than their physical counterpart.

This work will focus on the creation of a training system for ankle surgeries. Specifically, we will create guidance visualizations for the lateral opening wedge supramalleolar osteotomy. This surgery aims to fix ankle osteoarthritis by cutting and restructuring the tibia bone. We will design and evaluate several visualizations, that target to provide information, feedback, and evaluations on the starting point of the cut, the optimal orientation of the oscillating saw, and the required cutting depth. Another objective is to create an environment, in which trainees can perform this simulated ankle surgery and evaluate their performance independently.

2 Related Work

Several medical bone cutting simulators in VR exist already. Tsai et al. [THJ01] and Sofronia et al. [SDS12] proposed different visualization algorithms to create full-fledged bone cutting simulators. Their main goal is to create an alternative solution for training systems next to the conventional methods such as paper surgeries. The comparative study of Tsai et al. [THJ01] indicated that simulators allow surgeons to obtain more real and precise simulations about surgical procedures compared to paper-based simulations. In general, the implemented simulators allow students to hone their basic sawing skills and help surgeons in the preoperative planning stage.

Even though we have multiple works, which deal with the implementation of realistic bone cutting simulators, there are not many works about general surgical guidance and assistance with feedback visualizations in VR. Real-time evaluation-based visualization and feedback solutions for surgical applications are commonly explored in the Augmented Reality (AR) and mixed reality space.

Zhao et al. [ZXW+20] proposed an intelligent AR framework for neonatal endotracheal intubation training. They mentioned that trainees often have a limited understanding of practice trials due to the difficulty of identifying undesirable movements, which are merely based on trial outcomes. That is why usually training sessions rely on the feedback and evaluations of instructors. Their guidance visualization would provide imminent information and operation instructions, which leads to more independent skill acquisition and more training opportunities. The framework includes real-time guidance as well as performance evaluation visualizations, which are rendered to the Head Mounted Display (HMD).

In the case of AR guidance for osteotomies, Viehöfer et al. [VWZ+20] and Kiarostami et al. [KDR+20] focused their research on bone cutting guidance on different parts of the body. Viehöfer et al. [VWZ+20] investigated the efficiency and effectiveness of AR-based visualizations to improve the accuracy of the distal osteotomy during the hallux valgus surgery. For that, they projected an x-ray overlay onto a physical dummy foot. That overlay contains a cutting plane, which functions as a cutting guide. They compared the AR cut with a free hand cut made by experienced and inexperienced test surgeons. The work's conclusion was, that even though there was no significant performance difference for experienced surgeons, the overall performance of the less experienced testers was better when using the AR solution.

Kiarostami et al. [KDR+20] designed a guidance visualization in AR, which supports the user while performing the periacetabular osteotomy. Their research points were to confirm the feasibility, accuracy, and effect on the performance depending on the experience of using AR guidance. A chisel is used to cut through the sawbone pelvis. The guidance visualizes cutting planes at the correct spots on the pelvis. The surgeon can achieve an accurate cut by aligning the physical chisel over a projected chisel hologram. It indicates the optimal chisel position and rotation to perform the cut. The study of Kiarostami et al. [KDR+20] showed similar results to the ones of Viehöfer et al. [VWZ+20], where less experienced users significantly benefit from those types of visualizations. Additionally, they reported an increased accuracy while guided.

2 Related Work

Our work extends the above-mentioned research by creating a training system solely in virtual reality. Specifically, we will design and implement different guiding visualizations for the supramalleolar osteotomy.

3 Background: Supramalleolar Osteotomy

Before we can create a training system, that targets to assist the surgery of the ankle, we need to know more about the goals, that the surgery tries to achieve. This work in general will focus on techniques for the surgery correcting ankle osteoarthritis. Ankle osteoarthritis is a medical condition, which describes the occurrence of osteoarthritis in the ankle joint area [VHHF06]. The origin of ankle osteoarthritis is often due to alignment issues of the joints and the deformation of the ankle structure. This can typically lead to ankle pain and stiffness [AN06], [SCM03]. Common malalignments are valgus deformities (joints are pointing to the inside) and varus deformities (joints are pointing to the outside). Several surgical procedures such as the supramalleolar osteotomy are used as a treatment method in the early to mid-stages of ankle osteoarthritis [KH12]. Supramalleolar osteotomy is a surgery, which involves cutting and reshaping the structure of the bones in the foot-ankle area. A powerful broad oscillating saw is mainly used to perform cuts on the tibia or fibula bone of the leg [SCM03]. Depending on the malalignment type different osteotomy techniques are applied. There are the closing wedge and opening wedge procedures, which dictate whether we structure the bone by removing portions of the bone and closing it or opening it up and putting in an artificial bone graft. Then for each of those two procedures, there is a medial and lateral variation. They determine whether the operation should be positioned on the medial (inner) side or the lateral (outer) side of the leg. Fig. 3.1a shows the preoperative plan for the closing wedge procedure. The black line displays the current alignment of the hindfoot. The white line next to it is the target alignment, which can be obtained by cutting along the gray dashed lines and closing the bone together.



Figure 3.1: Supramalleolar Osteotomy: (a) Closing Wedge [CGOJ14a] (b) Opening Wedge [CGOJ14b]

3.1 Closing Wedge

The closing wedge supramalleolar osteotomy aims to correct the joint alignment by extracting a wedge of bone out of the tibia. The bone will then be closed and fixated with a staple, which stabilizes the osteotomy. This corrects the angle of the hindfoot relative to the tibia bone. To perform this operation the surgeons need to make two cuts horizontally to the tibia and fibula bone. In the preoperative planning, the needed correction angle is determined. With that, the surgeons know the starting points of both cuts and how far in the cut will be.

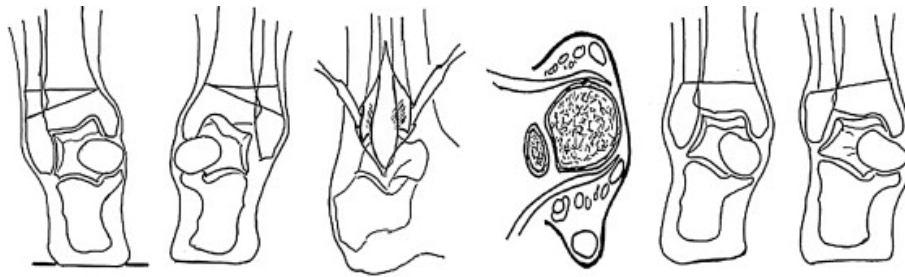


Figure 3.2: Closing Wedge Procedure [CGOJ14b]

3.2 Opening Wedge

In contrast to the closing wedge supramalleolar osteotomy, this technique only requires one cut horizontally to the bone. Therefore the surgeon only needs to know the starting point of the one cut and its total depth. After that, the bone will be opened and an artificial bone graft in form of a wedge is inserted into the gap. The wedge extends the length of the bone and will correct the alignment of the hindfoot.

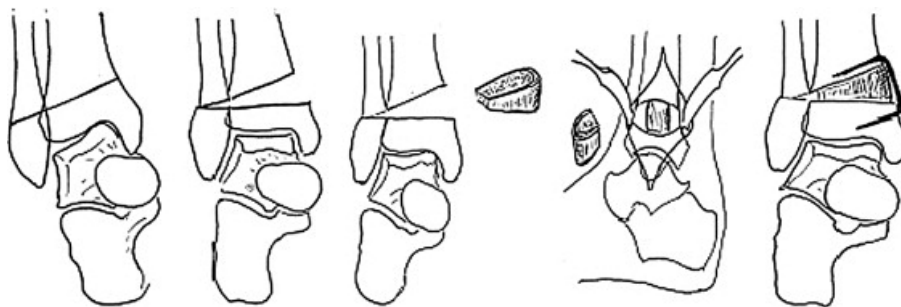


Figure 3.3: Opening Wedge Procedure [CGOJ14b]

4 Design Space

For this work, we specify essential requirements for creating a medical training system in virtual reality. The first one is the creation of a visualization, that supports and guides the user while performing the supramalleolar osteotomy, specifically the lateral opening wedge supramalleolar osteotomy. The second requirement is the repeatability and retrospective evaluation of the performed surgery, which allows to track the overall progression. To perform the lateral opening wedge supramalleolar osteotomy we need the following information beforehand:

1. The cutting line, which marks the start location of the cut
2. The orientation or angle of the cut/cutting plane
3. The target depth for each segment across the cutting line

The finished prototypes should include visualizations, that cover those mentioned points. Because there are multiple conditions that each prototype has to fulfill, we decided to break the visualization as a whole down into three subparts: the base, the depth, and the orientation. For each part, different visualizations are designed, that solely focus on supporting a small task, meaning the depth visualization concentrate on the current reached depth of the cut, and the orientation visualization concentrate on the angles and orientation of the saw blade and the cutting line. For the depth visualization, we introduce the On-Cut, Static-View, and Dynamic-View designs. The orientation visualizations are the Radial, Line-Projection, and Line-Caster. In the end all, parts are formed into one visualization for each possible combination. The total prototype count amounts to 9 (see Fig. 4.1).

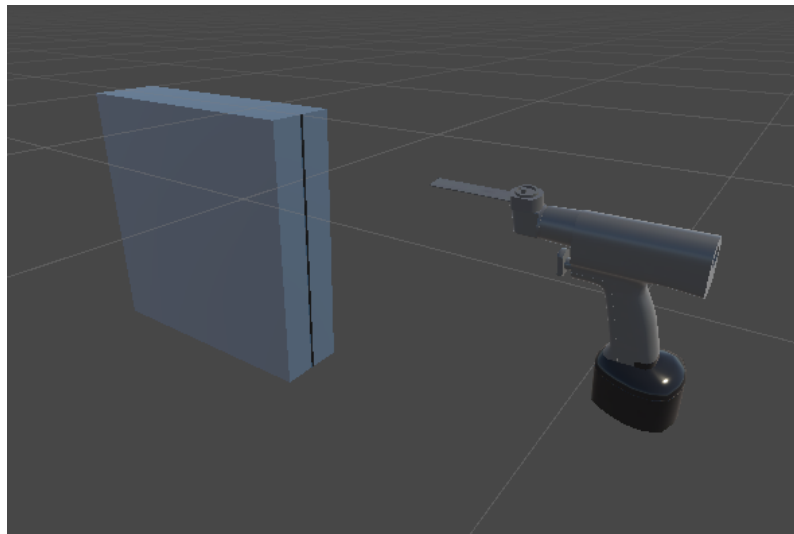
All prototypes are implemented with Unity Version 2020.3.3f1. The used virtual reality gear is the HTC VIVE Pro.

Orientation \ Depth	Radial	Line Projection	Line Caster
On Cut	Prototype 1	Prototype 2	Prototype 3
Static View	Prototype 4	Prototype 5	Prototype 6
Dynamic View	Prototype 7	Prototype 8	Prototype 9

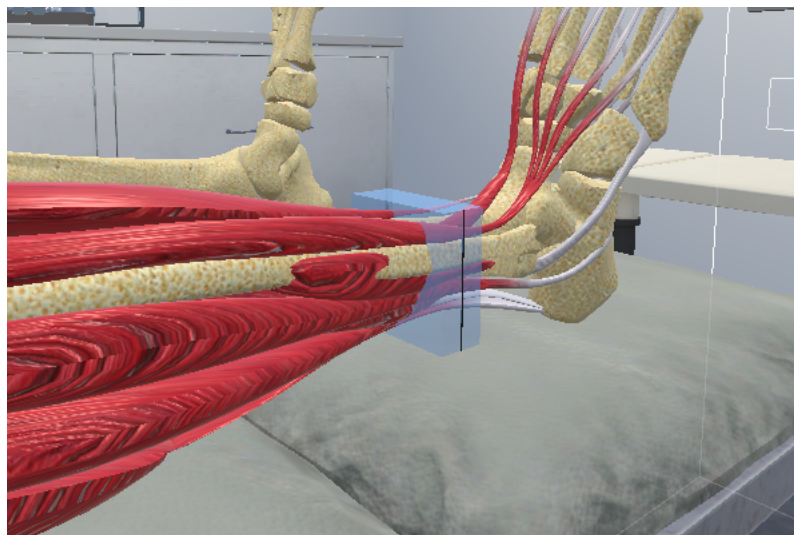
Table 4.1: Combinations of different visualizations

4.1 Base

This visualization is supposed to be used as a baseline for all prototypes. It incorporates a transparent box and the cutting line. The purpose of the box is to give the user the rough orientation and position of the cutting plane. The cutting line is black. It visualizes the entry point and length for the cut. Additionally, there is a grabbable 3D model of the oscillating saw, that is used for the surgery. To grab the saw the user has to point his controller and click on the 3D model. The saw will then attach to the hand of the user.



(a)



(b)

Figure 4.1: Base visualization: (a) The cutting box with the cutting line and the saw model. (b) The cutting box positioned onto a leg model.

4.2 Depth

4.2.1 On Cut

To indicate the current depth, this visualization takes the same approach as the crosshair prototype [HJLH19], which increases or decreases a circle indicator depending on the depth of the insertion. It is directly positioned onto the cutting line. In contrast to the needle insertion, this type of surgery does not only have one single entry point, but we have to deal with a saw blade, which has a set width. Also, this visualization should indicate the depth for all given segments of the cutting line. The On-Cut-Visualization uses bars, that expand depending on the reached depth of the saw blade. The widths of those bars are set to the length of the cutting line covered by the inserted saw blade. To set a maximum depth for each cutting line segment, there is a boundary curve on the outside edge. The closer the bars are to that boundary curve, the more accurate is the depth. To support this indication, the bars are color mapped regarding their distance to the boundary curve. Low accuracy is mapped to red and high accuracy is mapped to green as shown in Fig. 4.2.

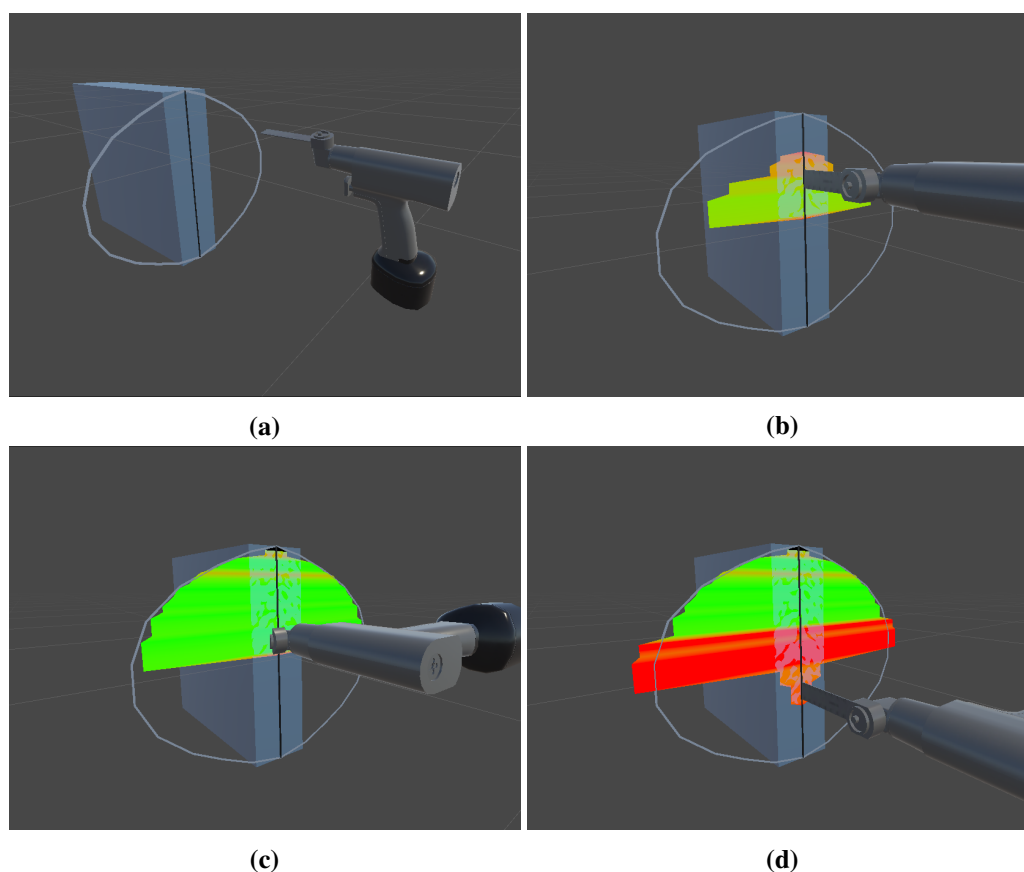


Figure 4.2: On-Cut-Visualization: (a) Gray ring represents the target boundary curve. (b) Bars are expanding when saw blade is inserted. (c) Green color mapping shows good depth accuracy. (d) Red color mapping for inaccurate depths.

4.2.2 Static View

The Static-View-Visualization is a live direct view to the cutting plane. It is comparable to an x-ray image, which is often used for preoperative planning and post-analysis of osteotomies. It enables the possibility to see the current depth of the saw blade inside the bone and the given target boundary curve, which sets the maximum depth. The already cut area is tracked and color mapped with green and red, depending on the depth accuracy. Furthermore, the user can move this view around the virtual world space and position it to their own preference.

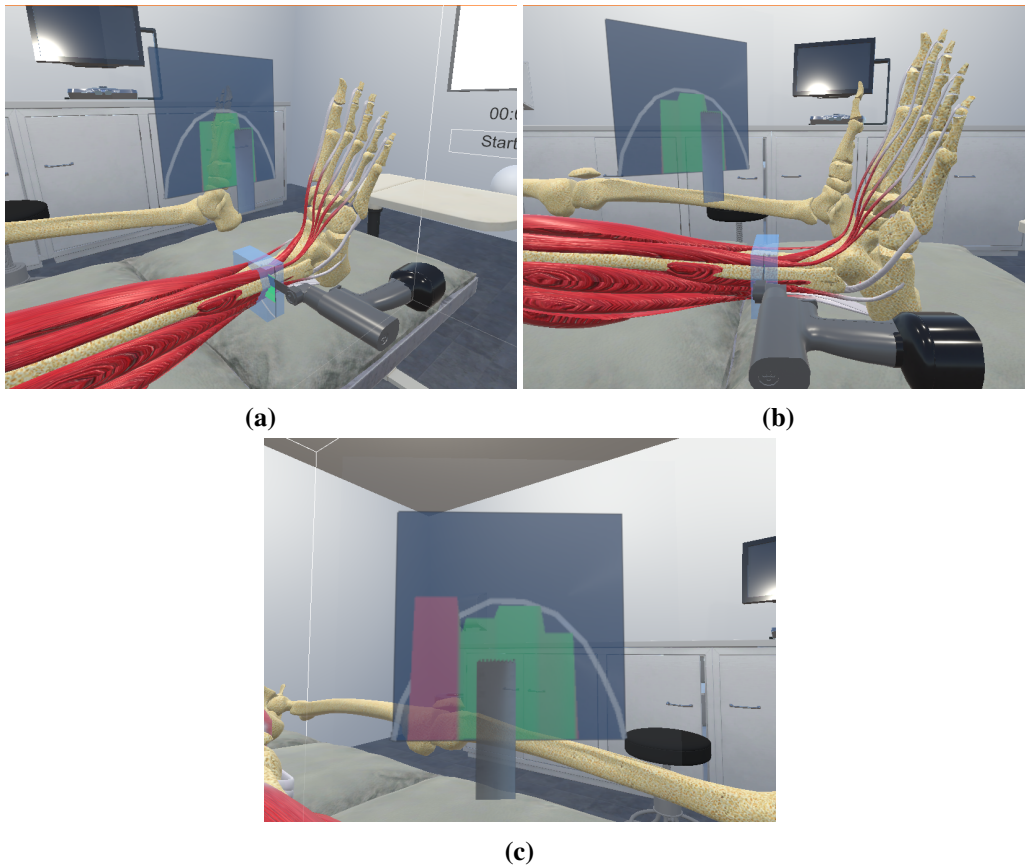


Figure 4.3: Static-View-Visualization: (a) Separate screen shows target boundary curve, the current depth and its curve. (b) The Screen is positioned with another angle. (c) Green-red color mapping for accurate-inaccurate depths.

4.2.3 Dynamic View

The Dynamic-View-Visualization is exactly built like the Static-View with one key difference. It implements the same x-ray view, but that view is bound to the HMD. That means this visualization will always be in the field of view of the user and it moves with the rotation of the user's viewpoint.

4.3 Orientation

4.3.1 Radial

The Radial-Visualization tracks the value difference between the target orientation/angle and saw blade angle. Let's define the axis, which has the same direction as the depth, as the z-axis. The axis, which is parallel to the cutting line is defined as the y-axis. The rotation difference around the z-axis is visualized by expanding and coloring a radial bar. The visualization y-axis is the same, but it utilizes a simple rectangular bar. If the saw blade rotation and target rotation differs strongly, both of these bars will increase in size, and their color changes from green to red. We deliberately allow the rotation around the x-axis, because that means the user can cut along the cutting plane by rotating the saw around that axis. This visualization is directly positioned onto the cutting line and orthogonal to the depth direction.

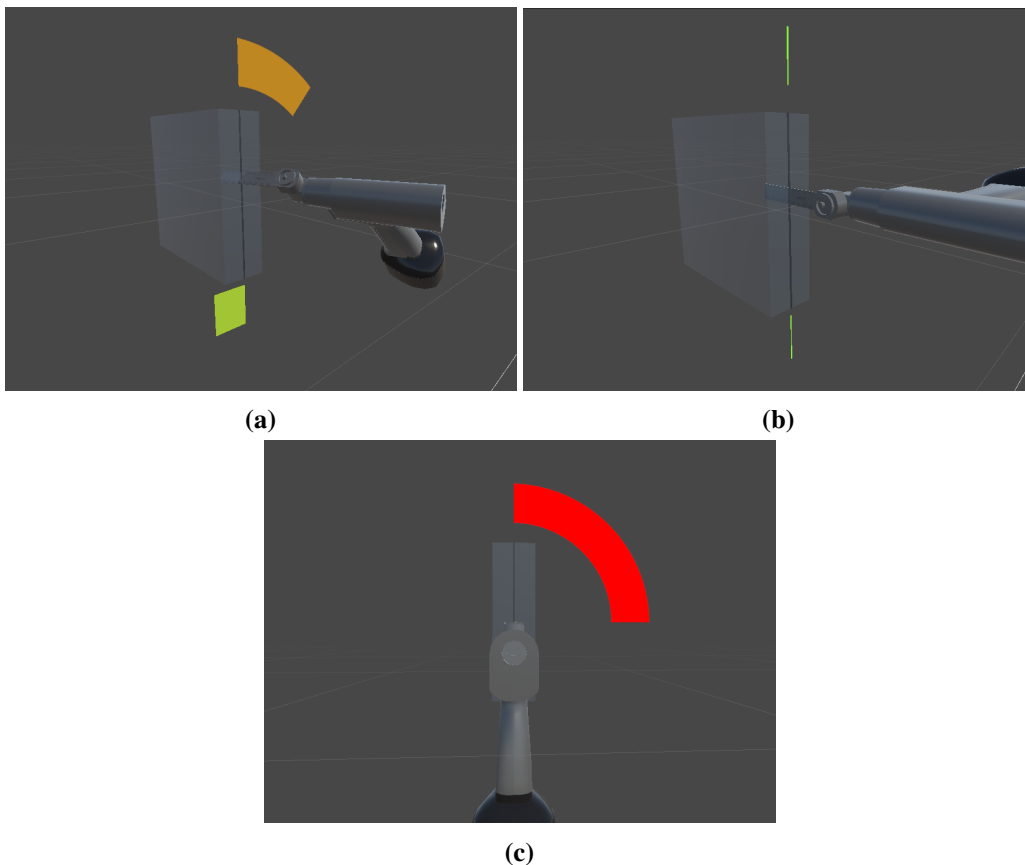


Figure 4.4: Radial-Visualization: (a) Angle differences between saw blade and cutting line, bars show the current rotation angles and are green-red color mapped. (b) Bars are nearly gone, which indicate a good orientation of the saw blade. (c) Front view, the saw blade angle difference is 90 degrees to the cutting line, the bar is colored red.

4.3.2 Line Projection

Just like the name suggests the Line-Projection-Visualization will project a line onto the plane that is orthogonal to the depth direction. The line is created by calculating two intersection points on the projecting plane. To determine those points we create orthogonal vectors between the saw blade tip corners and the projecting plane. The length of the line is the same as the width of the saw blade. Aligning the projected line with the cutting line will change its color from red to green. If the saw blade rotation is not the same as the target rotation, the projected line will be offset to the cutting line.

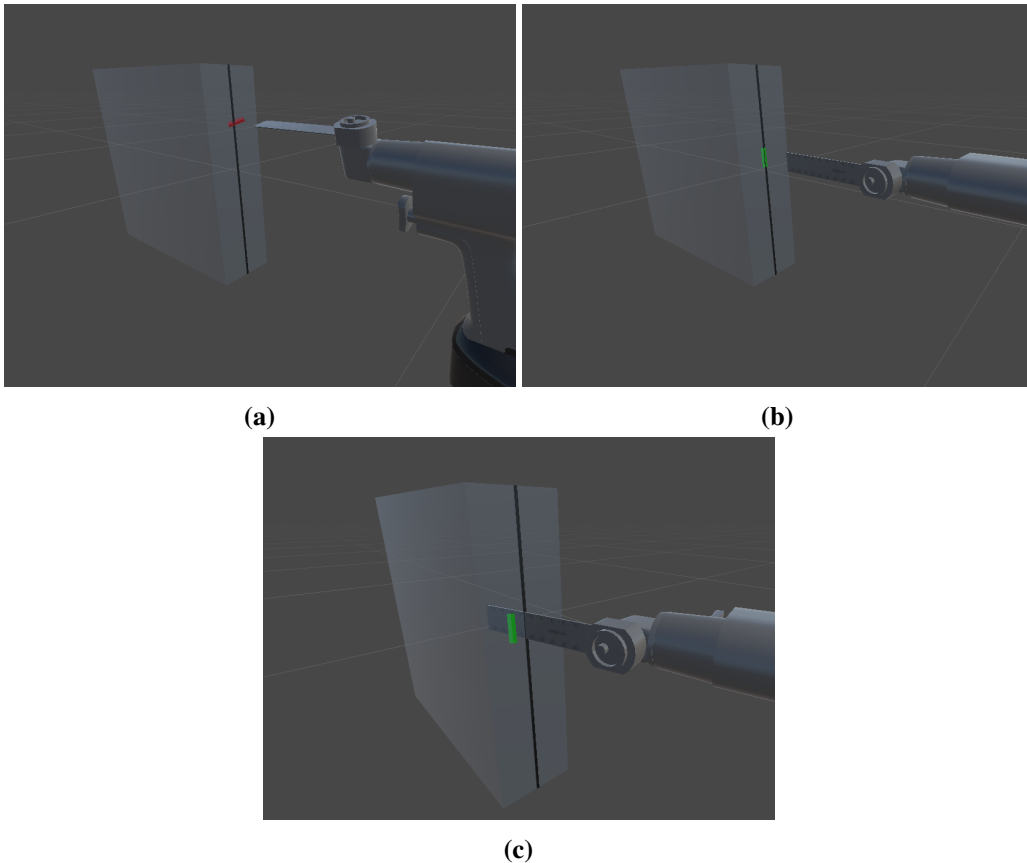


Figure 4.5: Line-Projection-Visualization: (a) A line is projected onto the cutting box, colored red because of the poor orientation of the blade. (b) Excellent alignment and orientation of the blade, green line is projected. (c) Inserted saw blade with poor orientation, green line is not aligned with the cutting line.

4.3.3 Line Caster

The Line-Caster-Visualization is an inverted variant of the Line-Projection-Visualization. It casts two lines from the corners of the saw blade tip to the projecting plane. From those intersection points, the cast lines are extended to both ends of the cutting line. Sometimes it is rather challenging to perceive depth and make positional assumptions in a virtual environment [GMB+18]. The cast lines should provide guidance in bringing the saw blade closer to the cutting line. Apart from that, the main functions such as angle offset and color mapping are identical to the Line-Projection.

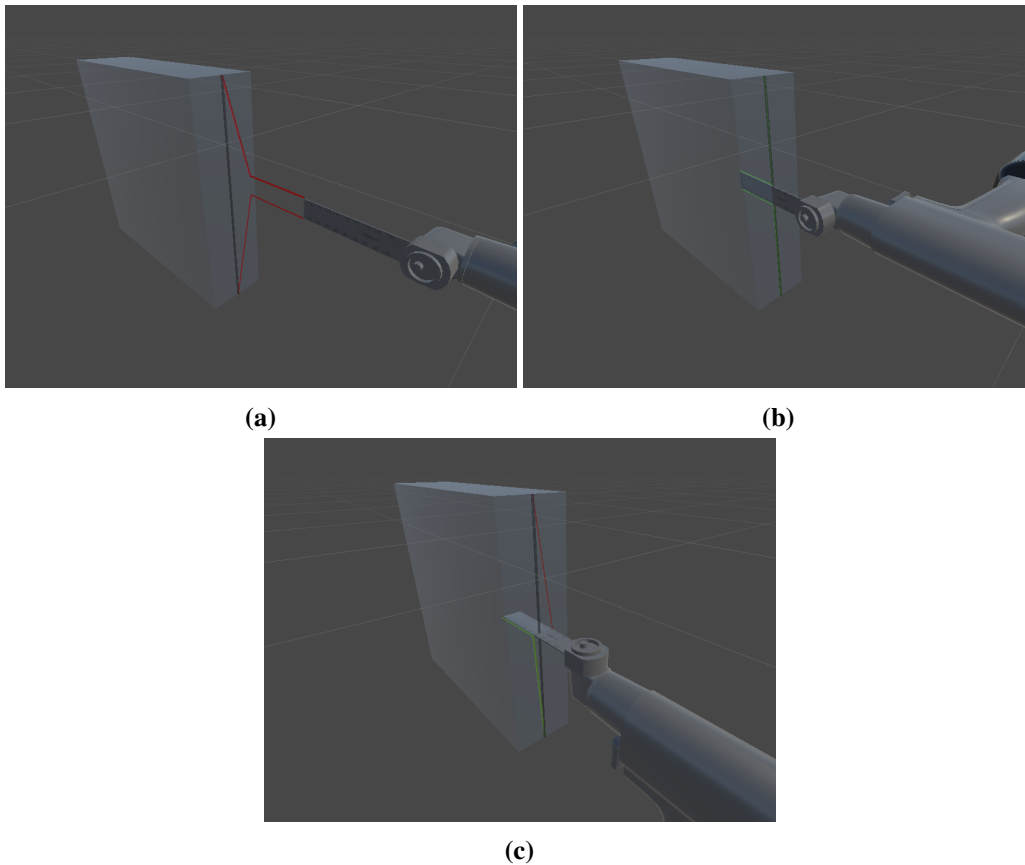


Figure 4.6: Line-Caster-Visualization: (a) Two lines are cast from the saw blade corners. (b) Excellent orientation and alignment of the inserted blade. (c) 90 degree blade angle to the cutting line.

4.4 Tracking the Cut and Post-Analysis

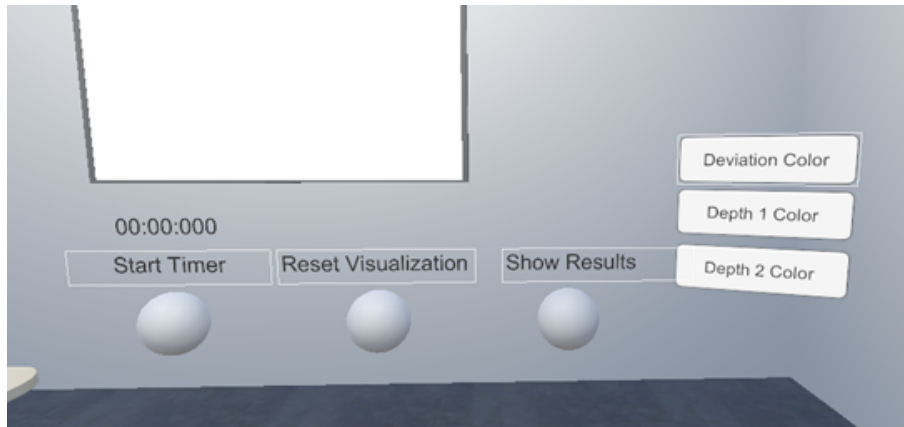


Figure 4.7: Training System Functionalities. Left: Timer to track operation time. Middle: Reset-Button to restart the operation. Right: Buttons for post-analysis.

In order to check how good the accuracy of the cut was, it is necessary to create some sort of system, which tracks the depth and orientation while the saw is in use. For that, we make use of generated 3D meshes. A mesh is a three-dimensional structure, which consists of many connected vertices. When the saw blade enters the cutting box, we will dynamically adjust the positions of each corresponding mesh vertex to the blade's deepest positions. The resulting cutting mesh visualizes the overall path of the saw blade.

A proper training system should provide functions to let trainees have the ability to evaluate their finished surgery and repeat the whole operation. For the post-analysis, we implemented a visualization, which is a scaled-up version of the cutting mesh with the set target boundary curve. The trainee can point their controllers to the mesh and rotate it around (see Fig. 4.9). That allows an open and detailed view on the deviation and depth of the finished cut. As shown in Fig. 4.8 it is also possible to map the mesh to different colors depending on whether the intention is to have a better look at the deviation or depth. Additionally, a simple timer and a clickable reset 3D object are created. The timer tracks the overall used time for the operation. The reset 3D object clears the cutting mesh and sets the surgery back to its starting point.

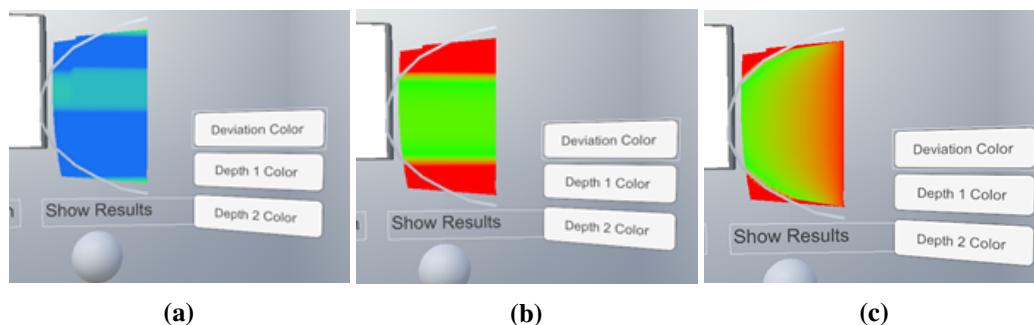


Figure 4.8: Scaled up cutting mesh (a) Color mapping for the deviation. (b) First color mapping for the depth. (c) Second color mapping for the depth.

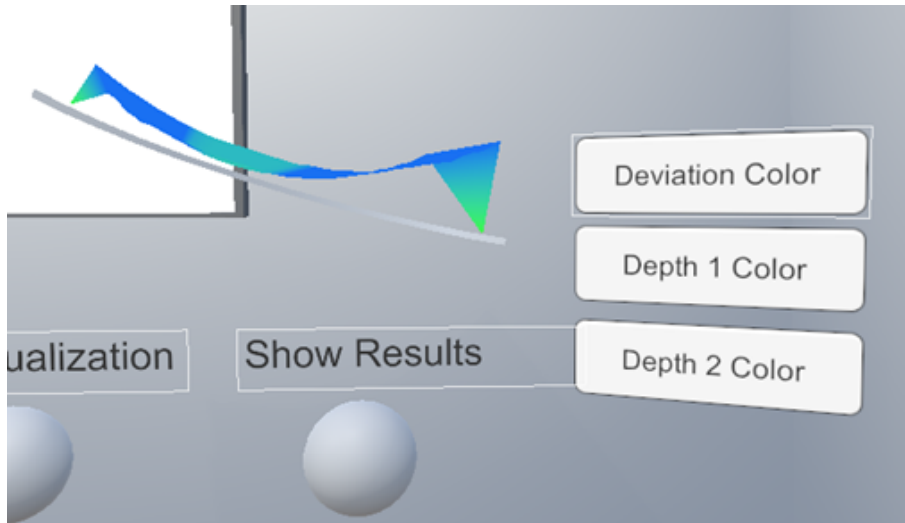


Figure 4.9: Rotated cutting mesh to allow for a better view on the deviation.

5 Preliminary Study

5.1 Accuracy

This section revolves around determining what the accuracy of a user-made cut should exactly be. After the user has finished a cut, a mesh will be created which represents the trajectory of the saw blade (see Section 4.4). An idea would be to compare the newly created cutting mesh against the desired target plane and look for deviation and depth differences.

5.1.1 Deviation

The deviation tells us how far we are deviating from the target cutting plane. The cutting mesh consists of several vertices and the distance to the plane is measured for each vertex. A large distance implicates a large deviation from the plane, which means the accuracy was far off. On the other hand, a small distance indicates good accuracy, because the cut was made close to the target plane.

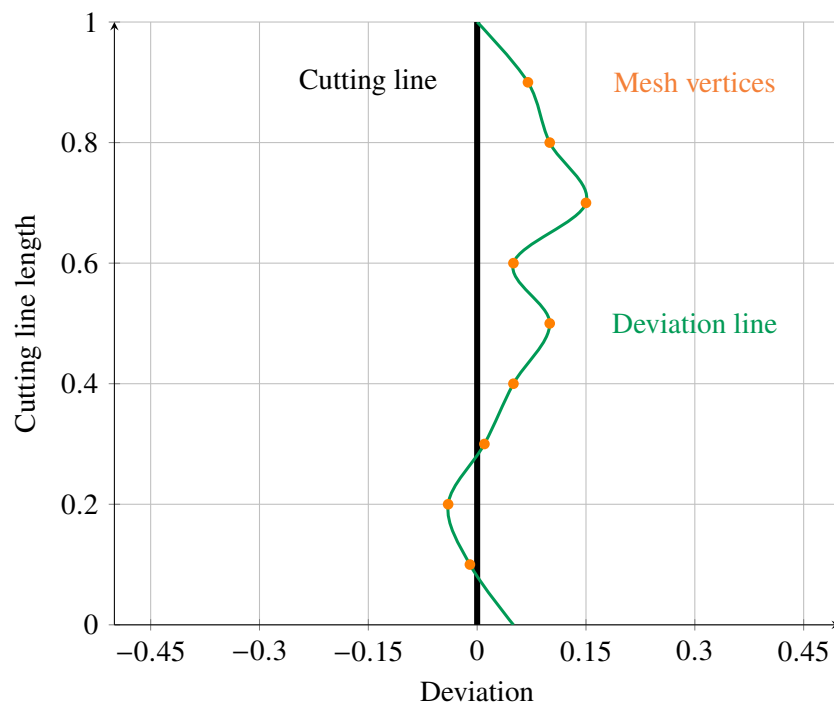


Figure 5.1: Example deviation from the cutting plane.

Min-Max-Average

We calculate the average, minimum, and maximum deviation by evaluating all absolute distances for each vertex. The minimum and maximum deviation are defined as the nearest and furthest distances to the cutting plane. To calculate the average deviation, we take all distances from each vertex and average them together.

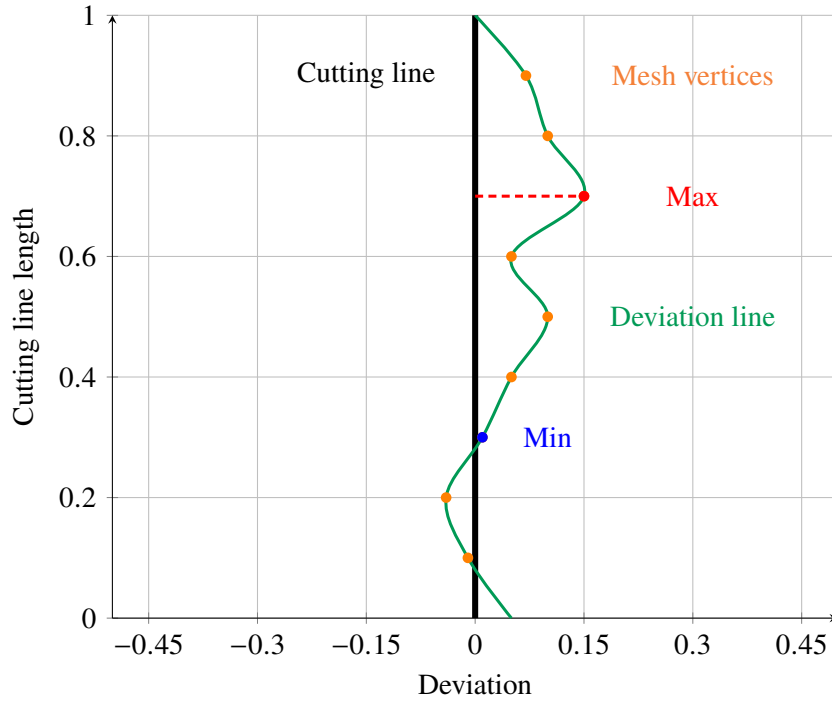


Figure 5.2: Minimum and maximum deviations of an example deviation line.

Formally, the equations are defined as

$$\text{deviation}_{\text{average}} = \frac{\sum_{i=1}^n |d_i|}{n}, \quad (5.1)$$

$$\text{deviation}_{\text{min}} = \min(|d_1|, |d_2|, \dots, |d_n|), \quad (5.2)$$

$$\text{deviation}_{\text{max}} = \max(|d_1|, |d_2|, \dots, |d_n|), \quad (5.3)$$

where d_i is the distance to the target cutting plane of vertex i and n is the total vertex count.

5.1.2 Positive Deviation

The target cutting plane divides the space into two separate sides. For that reason, it might viable to compute the average, minimum, and maximum for each side respectively. We define one side of the plane as the positive deviation and the other side as the negative deviation. That way it is possible to see if one side has more influence on the cut over the other one. To calculate the distance, we set distances of positions directly on the plane as the base value of 0. Vertices on the positive side have a positive offset, which results in a positive distance. The same applies to the vertices on the negative side, but with a negative offset. With that in mind, we can differentiate each side with their respective sign.

The adjusted equations for the positive side are

$$\text{deviation}_{\text{average,positive}} = \frac{\sum_{i=1}^n d_i}{n} \quad \text{with } d_i > 0, \quad (5.4)$$

$$\text{deviation}_{\text{min,positive}} = \min(d_1, d_2, \dots, d_n) \quad \text{with } d_i > 0, \quad (5.5)$$

$$\text{deviation}_{\text{max,positive}} = \max(d_1, d_2, \dots, d_n) \quad \text{with } d_i > 0. \quad (5.6)$$

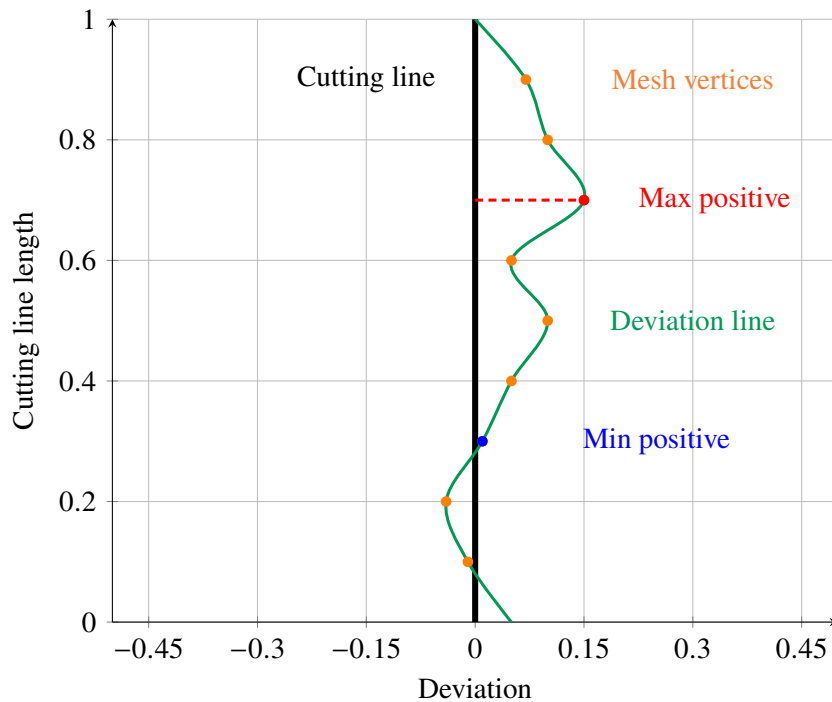


Figure 5.3: Minimum and maximum deviations for the positive side.

5.1.3 Negative Deviation

The distance of each vertex on the negative side is negative. Because of that reason, the minimum and maximum equations need to be switched. The adjusted equations for the negative side are:

$$\text{deviation}_{\text{average,negative}} = \frac{\sum_{i=1}^n d_i}{n} \quad \text{with } d_i < 0, \quad (5.7)$$

$$\text{deviation}_{\text{min,negative}} = \max(d_1, d_2, \dots, d_n) \quad \text{with } d_i < 0, \quad (5.8)$$

$$\text{deviation}_{\text{max,negative}} = \min(d_1, d_2, \dots, d_n) \quad \text{with } d_i < 0. \quad (5.9)$$

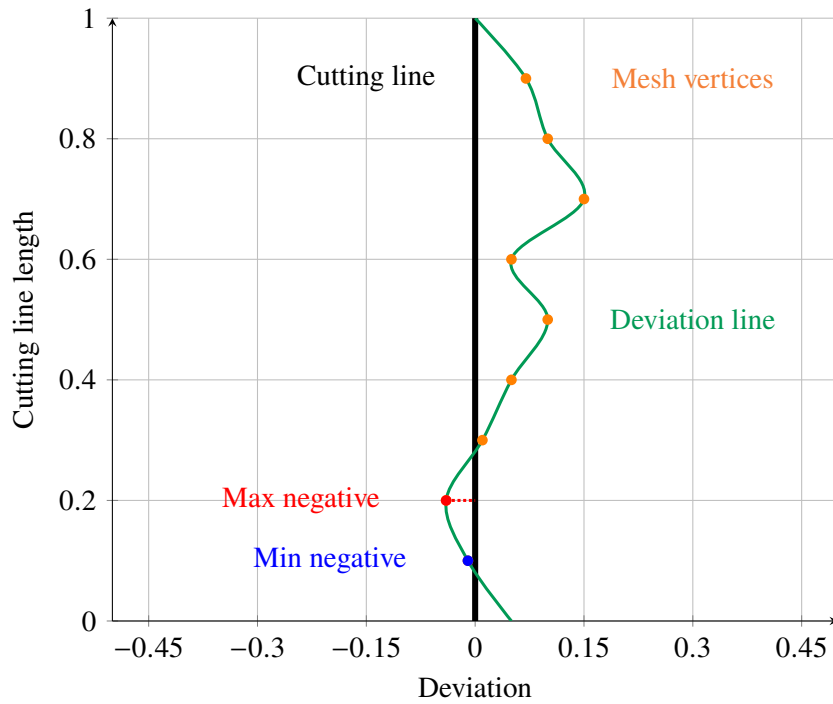


Figure 5.4: Minimum and maximum deviations for the negative side.

5.1.4 Depth

The depth describes how deep the user-made cut was. By the reason of a given predefined boundary curve, which is the target depth for each cutting line segment. The depth should both take the boundary curve and the deepness of the cut into consideration.

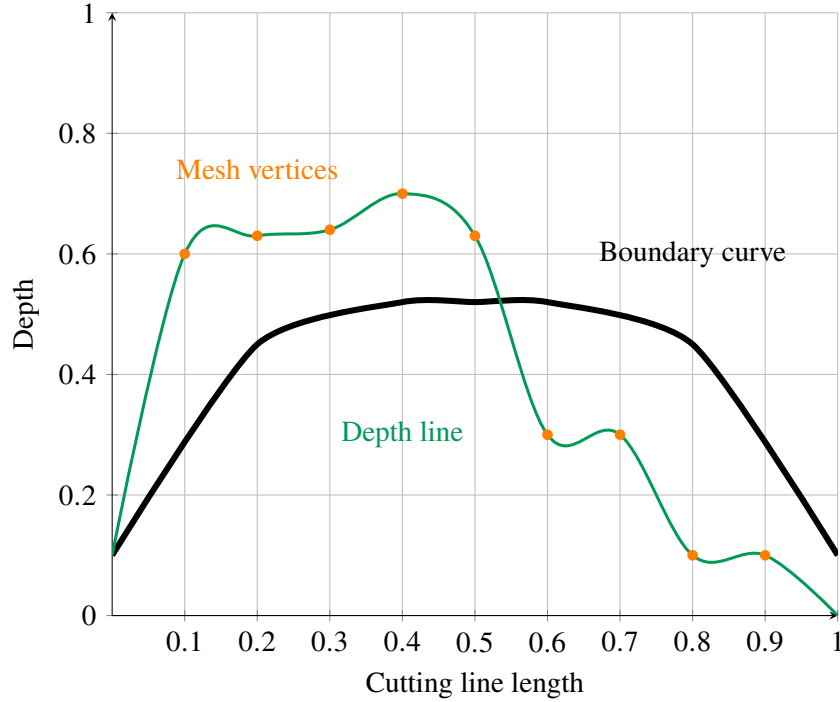


Figure 5.5: Example for depth of a made cut and the target boundary curve.

Min-Max-Average

Similar to the deviation calculations we also determine the minimum, maximum, and average depth for a user-made cut. First, vertices on the outer edge of the cutting mesh need to be sampled. They represent the deepest points of the cut along the cutting line. Then we compute the distance from each vertex point to the boundary curve.

$$\text{depth}_{\text{average}} = \frac{\sum_{i=1}^n |d_i|}{n}, \quad (5.10)$$

$$\text{depth}_{\text{min}} = \min(|d_1|, |d_2|, \dots, |d_n|), \quad (5.11)$$

$$\text{depth}_{\text{max}} = \max(|d_1|, |d_2|, \dots, |d_n|), \quad (5.12)$$

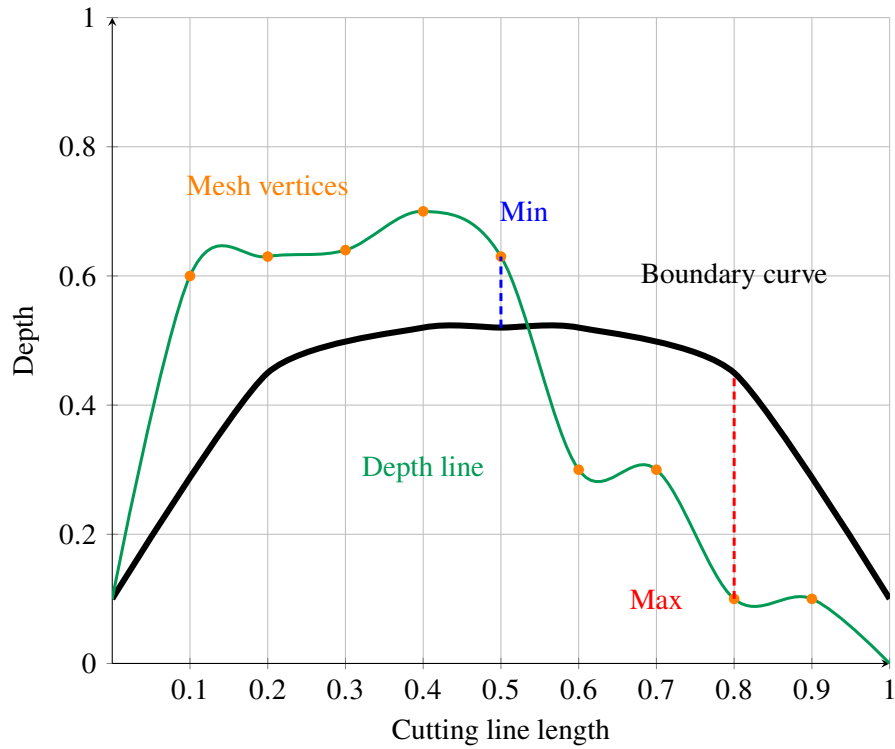


Figure 5.6: Minimum and maximum depth with sampled points on the made cut.

Overshoot and Undershoot

We define every vertex point that has a higher depth than the boundary curve as an overshooting point. Every point that did not reach the boundary curve is categorized as an undershooting point. For both types, we evaluate their minimum, maximum, and average depth. Additionally, we count all respective points and divide them by the total amount of sampled vertices. The equation for the overshoot and undershoot percentage are formally defined as:

$$\text{depth}_{\text{overshoot}\%} = \frac{\text{count}_{\text{overshoot}}}{n}, \quad (5.13)$$

$$\text{depth}_{\text{undershoot}\%} = \frac{\text{count}_{\text{undershoot}}}{n}, \quad (5.14)$$

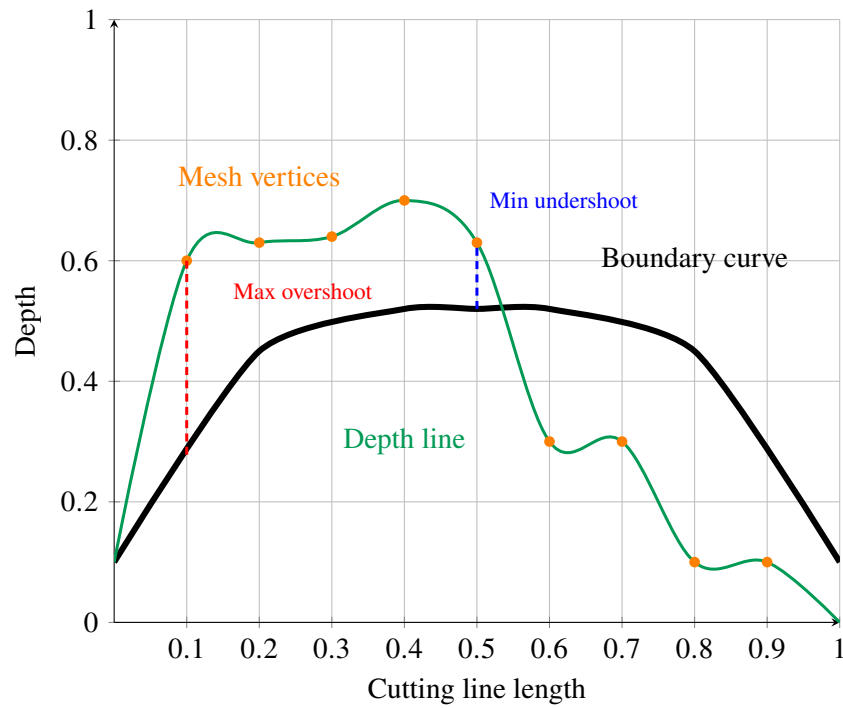


Figure 5.7: Minimum and maximum depth for overshooting points.

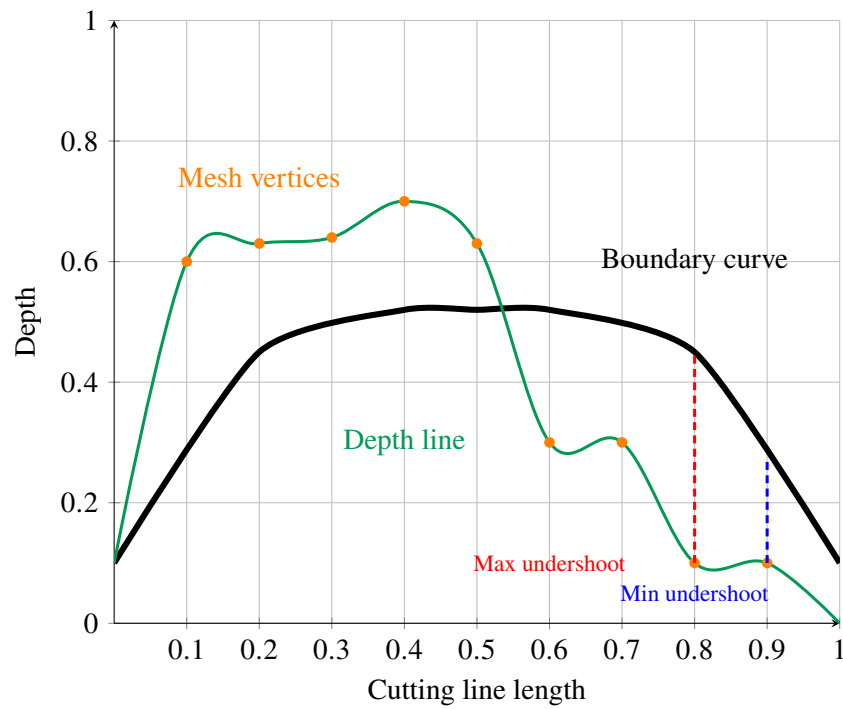


Figure 5.8: Minimum and maximum depth for undershooting points.

5.2 Study Design

Due to the limited time constraints of this project, we were only able to conduct a pilot study. We invited a medical expert to test and provide her assessment for each prototype. The first phase is the training phase. In this phase, the expert should get to know the virtual environment. It should provide an overview of the different mechanics, such as how to hold and use the saw and how to perform a simple cut. The second phase is the testing phase. The expert had to perform the cut for the lateral opening wedge supramalleolar osteotomy on all given prototypes. For that, we defined a randomized test order. The test sequence was as followed: Prototype 3, 4, 9, 8, 1, 5, 6, 2, 7. We specifically measured the accuracy information, which were introduced in Section 5.1.

Before each new prototype, the position, orientation of the cut, and the target boundary curve were randomized. To select a random target boundary curve we generated 140 probability curves from a skew-normal distribution with a Python script. The curves were created by using a different alpha value and sigma value each time. About 50 sampling points of the curve were then saved to a text file, so they could be recreated in the Unity environment. The position and orientation were randomized by sampling vector values from the Gaussian distribution with a small standard deviation.

5.3 Evaluation

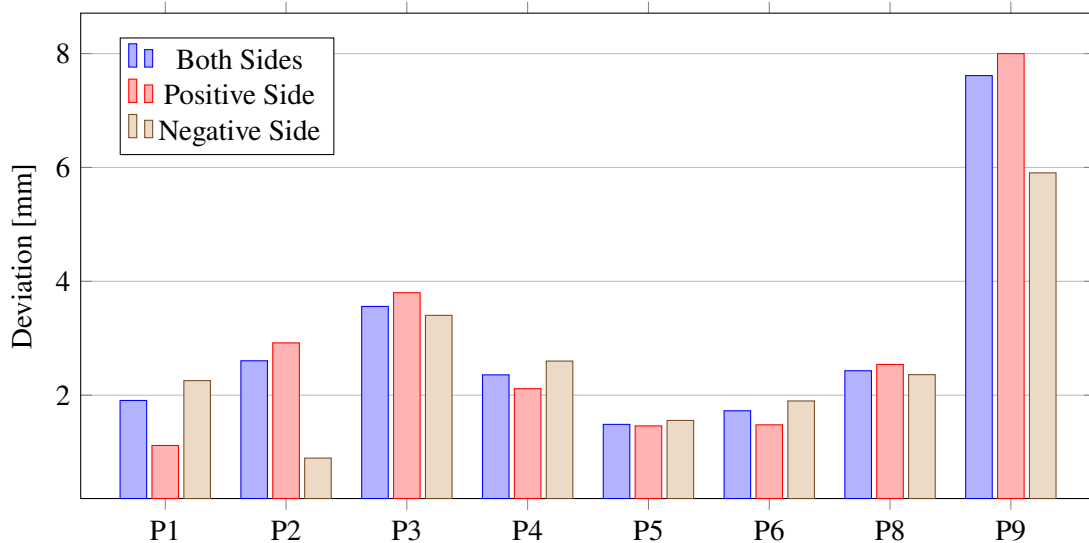


Figure 5.9: Average deviation of all tested prototypes.

Unfortunately, there were visualization errors during the test run for Prototype 7. The results for that prototype are not evaluated and are left out in these figures.

The average deviation range for Prototype 1 to Prototype 8 is between 1.5mm to 4mm, shown in Figure 5.9. Only Prototype 9 had a significantly higher average deviation at roughly 7.6mm. If we take a look at the deviations for the positive and negative sides, Prototype 2 and Prototype 9

had deviation differences of about 2mm. The differences for the other prototypes were rather slim. Overall Prototype 5, which implemented the Static-View and Line-Projection, performed the best with an average deviation of 1.48 mm.

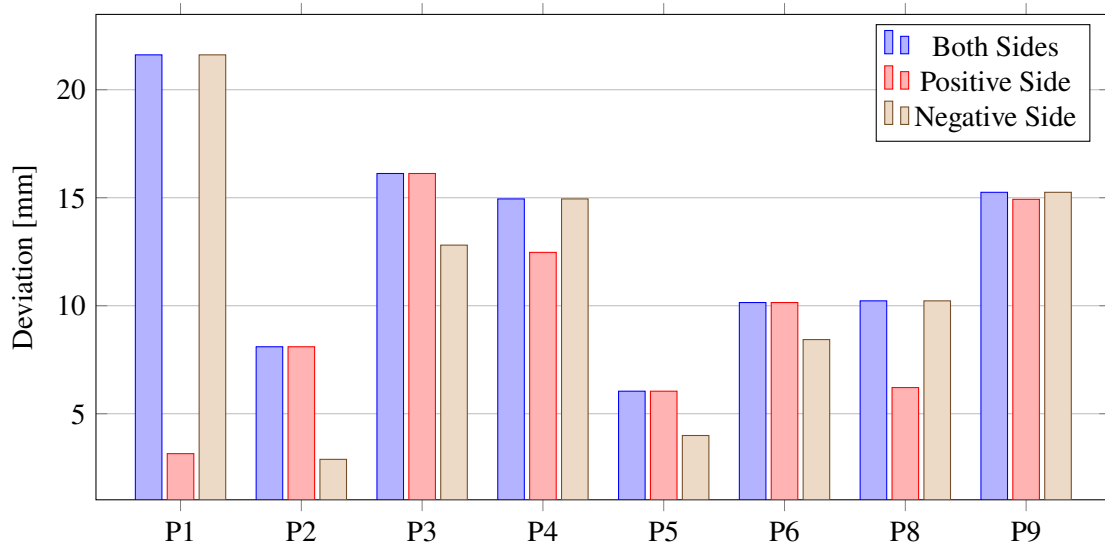


Figure 5.10: Maximum deviation of all tested prototypes.

Figure 5.10 shows the maximum deviation of all prototypes. The largest recorded maximum deviation was 21.6mm by Prototype 1. The other prototypes' max deviations ranged from 6mm to 16mm. Prototype 5 showed the smallest max deviation of 6mm.

In the case of the average depth, Prototype 1, 2, 3, 5, and 9 performed better than the others. Their average distances to the target boundary curve were the smallest with a range from 2mm to 4mm. The largest distance was achieved by Prototype 6 with an average distance of 11.8mm. Fig. 5.12 shows the maximum reached distance to the target boundary curve for each prototype. Again the same Prototypes that excelled in the average depth seem to have a good performance for the maximum distance as well. Fig. 5.11 and Fig. 5.12 show that for P4 to P9 the expert cut too far into the bone, meaning there is a higher overshoot distance.

According to the results, there is the indication that the prototypes, which implemented the visualizations directly on the cutting region, performed very well in both the deviation and depth of the cut.

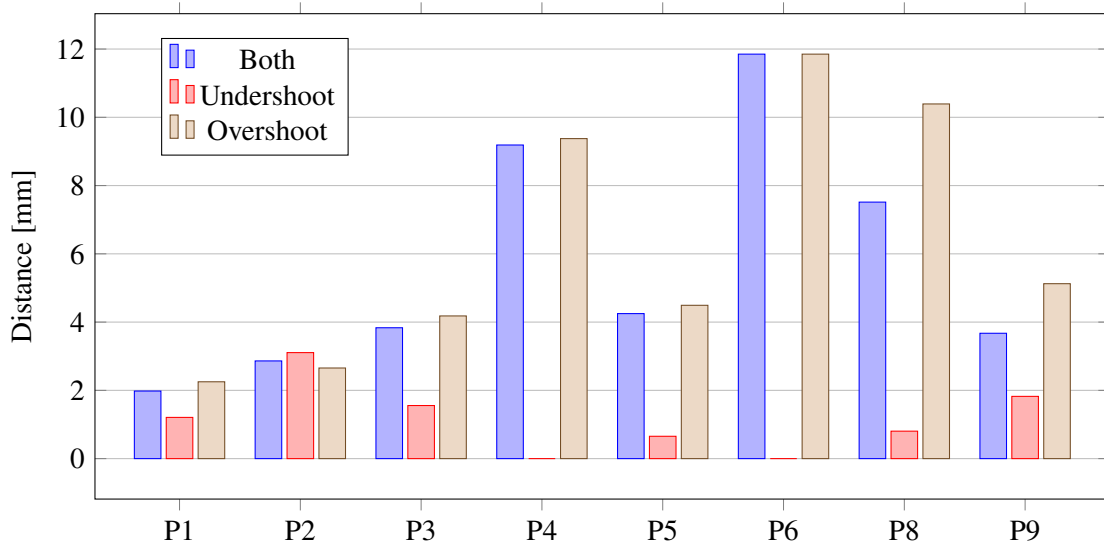


Figure 5.11: Average distances to the target boundary curve of all tested prototypes.

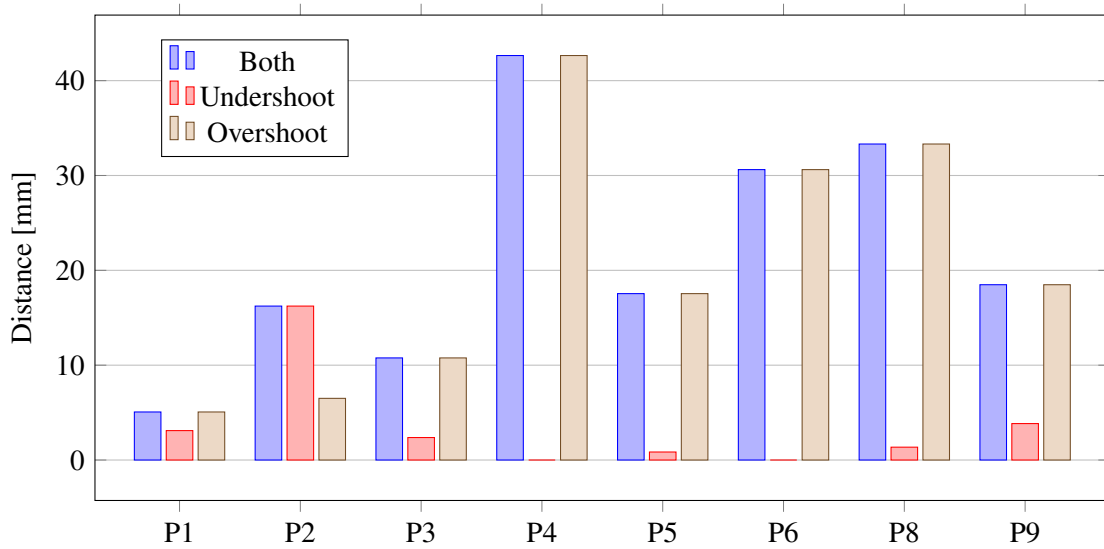


Figure 5.12: Maximum distances to the target boundary curve of all tested prototypes.

6 Discussion

All designs showed an improvement to the confidence of doctors by showing the coverage, the orientation, and the depth of the cut, through various visualizations. The overall tool could help with performance evaluation and improving training effects. Prototype 1, which included the On-Cut-Visualization and the Radial-Visualization was the most well-received prototype by the expert. An important observation was the performance difference between the prototypes that included the separate depth views (Static-View and Dynamic-View) and the On-Cut-Visualization. The expert told us in her feedback that it was rather difficult to focus on both the cutting location and the separate view due to the narrow field of view in VR. It makes sense because the user needs to constantly switch their gaze. A possible solution to this problem would be to position the depth visualization and orientation visualization in the same region, ideally somewhere right on the cutting region. Another point was the cutting box. Even though it provides some kind of rough estimation for the cutting region, it would be better to have it align with the surface of the physical leg model. Otherwise, it is difficult to mentally integrate the saw with the model. Also, the color maps and the various 3D lines need a rework for better visibility in VR. Due to the complexity of the prototypes, the user needs well-prepared tutorials and training to understand the designs.

In the process of designing and testing those visualizations, we noticed limitations regarding the gear and virtual environment in general. Sensors track the movement in real life and convert them to their virtual equivalent. Bad sensors can result in unstable movement tracking, which significantly impacts this kind of precise operation simulation. In the real-life or augmented environment, physical objects are used as the cutting dummy. Those objects exert resistance and provide stability to the inserted saw blade since they somewhat restrict the movements. In the virtual environment, all movements are more unrestricted. In the pilot study, we saw maximum deviations up to 2 centimeters, assuming one unit in VR equals to one meter in real life. This is generally unacceptable in a real operation. That is the reason why a perfect training system should have a precise bone cutting simulation with haptic feedback and simulated resistance while cutting. It would tremendously support high precision-based surgery simulations in virtual reality.

Of course, these results are only based on a preliminary study. We need a full comparative study to get a more detailed evaluation of each designed prototype.

7 Conclusion

Throughout this , we created a training system in virtual reality for ankle surgery, namely the supramalleolar osteotomy, which aims to provide an alternative training method for medical students. This training system incorporates a visual environment for the surgery and several functions to repeat and evaluate the performed operation. Additionally, we designed and investigated visualizations for guiding and assisting the surgeon during the operation. In the end, a total of 9 prototypes were created with different visualizations for the start, orientation, and coverage of the cut. A conducted pilot study with a medical expert showed that all designed prototypes were helpful and could improve the confidence of the surgeon. In general, guidance visualizations that were close to the cutting region performed the best. Overall the implemented tools for the training system had a positive impact on the training effects.

Outlook

This work only conducted a short preliminary study, which is not sufficient enough. A high priority is to have a full comparative study with all designed prototypes to identify further strengths and weaknesses of each visualization.

The expert also mentioned critique points. The visualizations should be reworked to have overall better visibility and mapping regarding their colorization.

Another point would be improving the simulation by adding haptic feedback and adjusting the algorithm to allow for a more precise cutting simulation. The created visualizations in VR could be eventually translated to AR to see whether they are suitable for such an environment. That would enable the possibility to use those guiding techniques not only in the context of a training system but in a real clinical surgery.

Acknowledgment

We thank MD. Ph.D. Suyuan Peng of the National Institute of Health Data Science, Peking University, for participating in the pilot study and providing valuable feedback.

Bibliography

- [AN06] N. Arden, M. C. Nevitt. “Osteoarthritis: Epidemiology”. In: *Best Practice & Research Clinical Rheumatology* 20.1 (2006). Osteoarthritis, pp. 3–25. ISSN: 1521-6942. DOI: <https://doi.org/10.1016/j.berh.2005.09.007>. URL: <https://www.sciencedirect.com/science/article/pii/S1521694205001087> (cit. on p. 17).
- [CGOJ14a] F. Colin, F. Gaudot, G. Odri, T. Judet. “Erratum to “Supramalleolar osteotomy: Techniques, indications and outcomes in a series of 83 cases” [Orthop. Traumatol. Surg. Res. 100 (2014) 413–18]”. In: *Orthopaedics & Traumatology: Surgery & Research* 100.5 (2014), p. 581. ISSN: 1877-0568. DOI: <https://doi.org/10.1016/j.otsr.2014.06.001>. URL: <https://www.sciencedirect.com/science/article/pii/S1877056814001248> (cit. on p. 17).
- [CGOJ14b] F. Colin, F. Gaudot, G. Odri, T. Judet. “Supramalleolar osteotomy: Techniques, indications and outcomes in a series of 83 cases”. In: *Orthopaedics & Traumatology: Surgery & Research* 100.4 (2014), pp. 413–418. ISSN: 1877-0568. DOI: <https://doi.org/10.1016/j.otsr.2013.12.027>. URL: <https://www.sciencedirect.com/science/article/pii/S1877056814000784> (cit. on pp. 17, 18).
- [GMB+18] N. Gerig, J. Mayo, K. Baur, F. Wittmann, R. Riener, P. Wolf. “Missing depth cues in virtual reality limit performance and quality of three dimensional reaching movements”. In: *PLOS ONE* 13 (Jan. 2018), e0189275. DOI: [10.1371/journal.pone.0189275](https://doi.org/10.1371/journal.pone.0189275) (cit. on p. 25).
- [HJLH19] F. Heinrich, F. Joeres, K. Lawonn, C. Hansen. “Comparison of Projective Augmented Reality Concepts to Support Medical Needle Insertion”. In: *IEEE Transactions on Visualization and Computer Graphics* 25.6 (2019), pp. 2157–2167. DOI: [10.1109/TVCG.2019.2903942](https://doi.org/10.1109/TVCG.2019.2903942) (cit. on p. 21).
- [KDR+20] P. Kiarostami, C. Dennler, S. Roner, R. Sutter, P. Fürnstahl, M. Farshad, S. Rahm, P. Zingg. “Augmented reality-guided periacetabular osteotomy—proof of concept”. In: *Journal of Orthopaedic Surgery and Research* 15 (Nov. 2020). DOI: [10.1186/s13018-020-02066-x](https://doi.org/10.1186/s13018-020-02066-x) (cit. on p. 15).
- [KH12] M. Knupp, B. Hintermann. “Treatment of Asymmetric Arthritis of the Ankle Joint with Supramalleolar Osteotomies”. In: *Foot & Ankle International* 33.3 (2012). PMID: 22734290, pp. 250–252. DOI: [10.3113/FAI.2012.0250](https://doi.org/10.3113/FAI.2012.0250). eprint: <https://doi.org/10.3113/FAI.2012.0250>. URL: <https://doi.org/10.3113/FAI.2012.0250> (cit. on p. 17).
- [RK05] A. Rizzo, G. J. Kim. “A SWOT Analysis of the Field of Virtual Reality Rehabilitation and Therapy”. In: *Presence* 14.2 (2005), pp. 119–146. DOI: [10.1162/1054746053967094](https://doi.org/10.1162/1054746053967094) (cit. on p. 13).

- [SCM03] E. D. Stamatis, P. S. Cooper, M. S. Myerson. “Supramalleolar Osteotomy for the Treatment of Distal Tibial Angular Deformities and Arthritis of the Ankle Joint”. In: *Foot & Ankle International* 24.10 (2003). PMID: 14587989, pp. 754–764. DOI: [10.1177/107110070302401004](https://doi.org/10.1177/107110070302401004). eprint: <https://doi.org/10.1177/107110070302401004>. URL: <https://doi.org/10.1177/107110070302401004> (cit. on p. 17).
- [SDS12] R. E. Sofronia, A. Davidescu, G. G. Savii. “Towards a Virtual Reality Simulator for Orthognathic Basic Skills”. In: *Mechanisms, Mechanical Transmissions and Robotics*. Vol. 162. Applied Mechanics and Materials. Trans Tech Publications Ltd, Apr. 2012, pp. 352–357. DOI: [10.4028/www.scientific.net/AMM.162.352](https://doi.org/10.4028/www.scientific.net/AMM.162.352) (cit. on p. 15).
- [THJ01] M.-D. Tsai, M.-S. Hsieh, S.-B. Jou. “Virtual reality orthopedic surgery simulator”. In: *Computers in Biology and Medicine* 31.5 (2001), pp. 333–351. ISSN: 0010-4825. DOI: [https://doi.org/10.1016/S0010-4825\(01\)00014-2](https://doi.org/10.1016/S0010-4825(01)00014-2). URL: <https://www.sciencedirect.com/science/article/pii/S0010482501000142> (cit. on p. 15).
- [VHHF06] V. Valderrabano, B. Hintermann, M. Horisberger, T. S. Fung. “Ligamentous Post-traumatic Ankle Osteoarthritis”. In: *The American Journal of Sports Medicine* 34.4 (2006). PMID: 16303875, pp. 612–620. DOI: [10.1177/0363546505281813](https://doi.org/10.1177/0363546505281813). eprint: <https://doi.org/10.1177/0363546505281813>. URL: <https://doi.org/10.1177/0363546505281813> (cit. on p. 17).
- [VWZ+20] A. Viehöfer, S. Wirth, S. Zimmermann, L. Jaberg, C. Dennler, P. Fürnstahl, M. Farshad. “Augmented reality guided osteotomy in hallux Valgus correction”. In: *BMC Musculoskeletal Disorders* 21 (June 2020). DOI: [10.1186/s12891-020-03373-4](https://doi.org/10.1186/s12891-020-03373-4) (cit. on p. 15).
- [ZXW+20] S. Zhao, X. Xiao, Q. Wang, X. Zhang, W. Li, L. Soghier, J. Hahn. “An Intelligent Augmented Reality Training Framework for Neonatal Endotracheal Intubation”. In: *2020 IEEE International Symposium on Mixed and Augmented Reality (ISMAR)*. 2020, pp. 672–681. DOI: [10.1109/ISMAR50242.2020.00097](https://doi.org/10.1109/ISMAR50242.2020.00097) (cit. on p. 15).

All links were last followed on March 1, 2022.

Declaration

I hereby declare that the work presented in this thesis is entirely my own and that I did not use any other sources and references than the listed ones. I have marked all direct or indirect statements from other sources contained therein as quotations. Neither this work nor significant parts of it were part of another examination procedure. I have not published this work in whole or in part before. The electronic copy is consistent with all submitted copies.

place, date, signature